Inorg. Chem. **2003**, *42*, 5244–5251

DFT Calculations of Isomer Shifts and Quadrupole Splitting Parameters in Synthetic Iron–Oxo Complexes: Applications to Methane Monooxygenase and Ribonucleotide Reductase

Tiqing Liu,* Timothy Lovell,* Wen-Ge Han, and Louis Noodleman*

Department of Molecular Biology, TPC-15, The Scripps Research Institute, La Jolla, California 92037

Received October 24, 2002

To predict isomer shifts and quadrupole splitting parameters of Fe atoms in the protein active sites of methane monooxygenase and ribonucleotide reductase, a correlation between experimental isomer shifts ranging 0.1–1.5 mm s^{-1} for Fe atoms in a training set with the corresponding density functional theory (DFT) calculated electron densities at the Fe nuclei in those complexes is established. The geometries of the species in the training set, consisting of synthetic polar monomeric and dimeric iron complexes, are taken from the Cambridge structural database. A comparison of calculated Mössbauer parameters for Fe atoms from complexes in the training set with their corresponding experimental values shows very good agreement (standard deviation of 0.11 mm/s, correlation coefficient of –0.94). However, for the Fe atoms in the active sites of the structurally characterized proteins of methane monooxygenase and ribonucleotide reductase, the calculated Mössbauer parameters deviate more from their experimentally measured values. The high correlation that exists between calculated and observed quadrupole splitting and isomer shift parameters for the synthetic complexes leads us to conclude that the main source of the error arising for the protein active sites is due to the differing degrees of atomic-level resolution for the protein structural data, compared to the synthetic complexes in the training set. Much lower X-ray resolutions associated with the former introduce uncertainty in the accuracy of several bond lengths. This is ultimately reflected in the calculated isomer shifts and quadrupole splitting parameters of the Fe sites in the proteins. For the proteins, the closest correspondence between predicted and observed Mössbauer isomer shifts follows the order $MMOH_{red}$, RNR_{red}, $MMOH_{ox}$, and RNR_{ox}, with average deviations from experiment of 0.17, 0.17, 0.17–0.20, and 0.32 mm/s, but this requires DFT geometry optimization of the iron–oxo dimer complexes.

1. Introduction

Iron, with its large bioavailability, is an essential element for life on planet Earth.[1] As a consequence, iron is incorporated into many proteins and enzymes that perform critical biochemical functions.[2] Among the binuclear non-heme iron proteins,[3] methane monooxygenase (MMO) and ribonucleotide reductase (RNR) are well-known, with the hydroxylase component of MMO (MMOH) catalyzing methane oxidation[4,5] while RNR plays a key role in the synthesis of deoxyribonucleotides required by all living organisms.[6,7]

On the atomic level, MMO and RNR have strikingly similar active sites, and during the course of their distinct chemistries, it is clear that there are significant mechanistic elements in common over their reaction paths. Differences arise in the active site reactivity with molecular oxygen, which constitutes a first branch point in the subsequent chemical reactions. After this reaction branching, the catalytic

* To whom correspondence should be addressed. E-mail: lou@scripps.edu (L.N.).

(1) Greenwood, N. N.; Earnshaw, A. In *Chemistry of the Elements*, 2nd Edition; Oxford University Press: New York, 2002.
(2) Holm, R. H.; Kennepohl, P.; Solomon, E. I. *Chem. Rev.* **1996**, *96*, 2239.
(3) Solomon, E. I.; Brunold, T. C.; Davis, M. I.; Kemsley, J. N.; Lee, S.-K.; Lehnert, N.; Neese, F.; Skulan, A. J.; Yang, Y.-S.; Zhou, J. *Chem. Rev.* **2000**, *100*, 235.
(4) Rosenzweig, A. C.; Nordlund, P.; Takahara, P. M.; Frederick, C. A.; Lippard, S. J. *Chem. Biol.* **1995**, *2*, 409.
(5) (a) Elango, N.; Radhakrishnan, R.; Froland, W. A.; Wallar, B. J.; Earhart, C. A.; Lipscomb, J. D. Olendorf, D. O. *Protein Sci.* **1997**, *6*, 556. (b) Rosenzweig, A. C.; Frederick, C. A.; Lippard, S. J.; Nordlund, P. *Nature* **1993**, *366*, 537.
(6) Reichard, P. *Science* **1993**, *260*, 1773.
(7) Stubbe, J.; van der Donk, W. A. *Chem. Rev.* **1998**, *98*, 705.

10.1021/ic020640y CCC: $25.00
Published on Web 07/31/2003

mechanisms by which these two proteins perform their unique functions remain only partially understood at present, mostly because the highly prized structures of the key catalytic intermediates, which enable these two proteins to bring about different chemical reactions, are not yet known. A direct measure of the important structural elements of these key intermediates can be obtained by protein crystallography, but a major obstacle presented to this technique is that the key intermediates are very short-lived and it is difficult to stabilize the protein on a sufficiently long time scale to obtain crystals for diffraction studies. The catalytic mechanisms of MMO and RNR are therefore not trivial to follow with a direct structural probe.

Spectroscopy generally provides a means of following catalytic reactions for which the structures of short-lived intermediates are not available. Mössbauer spectroscopy[8,9] typically takes hours or days for an accurate measurement of a biological sample, but the situation can be remedied somewhat by using the freeze−quench approach, which allows trapping of unstable and otherwise short-lived species.[10] Measured parameters such as isomer shift, quadrupole splitting, and metal and ligand hyperfine for ^{57}Fe sites then enable an indirect measure of many factors such as metal oxidation and spin state, the local chemical environment at the iron site, the electric field gradient, the occupation of iron d levels, and the degree of valence delocalization in mixed-valence systems. In combination with other spectroscopic techniques, these parameters allow models for the key intermediates to be proposed and they also represent a yardstick by which postulated models and existing protein structural data can be examined and compared with known synthetic analogues and, therefore, gauged in a qualitative fashion.

The goal of this paper is to predict accurate isomer shifts (and also quadrupole splittings) on the basis of calculated electron densities and electric field gradients at the iron nuclei[11,12] using density functional theory.[13] From fundamental physical principles, the isomer shift δ, with respect to a reference system for a Mössbauer atom (^{57}Fe), is linearly proportional to the changes in electronic density at the nucleus (defined here as *nuclear density*) that arise due to the variations in the electron density from the iron valence orbitals plus inner shells, mainly iron 4s and indirectly the 3d, by polarizing valence 4s and subvalence 3s. The quadrupole splitting parameter ΔE_Q of an atom is also highly sensitive to the surrounding chemical environment and consequently to valence and lattice contributions to the electric field gradient.[14,16,17] ΔE_Q is proportional to the nuclear quadrupole moment, which for ^{57}Fe of $I = 3/2$ has a best current value of 0.15 b (barns).[15,16] In previous work, Dufek et al.[17] derived a value of 0.17 barns from state of the art DFT calculations for crystalline samples. The difference of 0.02 barns (13%) serves to illustrate the degree of uncertainty associated with values currently used for the nuclear quadrupole moment.

To calculate isomer shifts and quadrupole splitting parameters of Fe atoms in protein active sites, a correlation between experimental isomer shifts ranging from 0.1 to 1.5 mm s^{-1} for Fe atoms in a known training set of complexes with the corresponding electron densities at the Fe nuclei in those complexes must first be established and then validated. That the (μ-oxo)diiron (Fe−O−Fe) and (μ-hydroxo)diiron (Fe−OH−Fe) units appear consistently in a number of dinuclear non-heme iron proteins is to our advantage, and accordingly, the training set we have chosen to establish our correlation incorporates a range of synthetic dimeric iron complexes that display these structural features, as well as polar monomeric iron species. For all structures in the training set, measured isomer shift and quadrupole splitting data are available (see Table 1 of this work) and allow the building of a linear relationship between the isomer shifts of Fe atoms for the synthetic complexes with their corresponding calculated nuclear densities (and for calculated and observed quadrupole splittings).

After verification that a linear relationship exists between experimental isomer shifts and the calculated nuclear densities and that there is a close correspondence between calculated and observed quadrupole splittings as well for the synthetic systems of the training set, the reliability of our predictive methodology as applied to proteins is gauged. Calculated isomer shifts and quadrupole splitting parameters for the structurally characterized oxidized and reduced protein active sites of MMO[18] and RNR[19] are compared and contrasted with those values experimentally determined. In doing so, the accuracy of existing X-ray data for oxidized and reduced MMO and RNR is assessed in a qualitative manner by comparison both with DFT geometry optimized structures and spectroscopic indicators of active site structure.

2. Computational Details

2.1. ADF Calculations. The Amsterdam density functional package[20] (ADF, version 2002.02) was employed to compute energies of the active site clusters. The ADF basis set IV with all electrons included in the calculations (no frozen cores) was used to model Fe atoms and basis set IV for the

(8) Gütlich, P.; Ensling, J. *Inorganic Electronic Structure and Spectroscopy*; John Wiley and Sons: New York, 1999; Vol. I, pp 161−212.
(9) Gütlich, P.; Link, R.; Trautwein, A. X. *Mössbauer Spectroscopy and Transition Metal Chemistry*; Springer-Verlag: Berlin, 1978.
(10) Huynh, B.-H.; Bollinger, J. M., Jr.; Edmondson, D. E. In *Spectroscopic methods in bioinorganic chemistry*; Solomon, E. I., Hodgson, K. O., Eds.; ACS Symposium Series 692; Oxford University Press: New York, **1998**; pp 403−422.
(11) Noodleman, L.; Norman, J. G., Jr.; Osbourne, J. H.; Aizan, A.; Case, D. A. *J. Am. Chem. Soc*. **1985**, *107*, 3418.
(12) Nemykin, V. N.; Kobayashi, N.; Chenii, V. Y.; Belksy, V. K. *Eur. J. Inorg. Chem*. **2001**, *3*, 733.
(13) Ziegler, T. *Chem. Rev*. **1991**, *91*, 651 and references therein.
(14) Liu, T.; Case, D. A.; Noodleman, L. Calculations of quadrupole splitting parameters of iron in iron−sulfur analogues and complexes by density functional theory. Manuscript in preparation.
(15) Martínez-Pinedo, G.; Schderdtfeger, P.; Caurier, E.; Langanke, K.; Nazarewicz, W. Söhnnel, T. *Phys. Rev. Lett.* **2001**, *87*, 062701.
(16) Lauer, S.; Marathe, V. R.; Trautwein, A. X. *Phys. Rev. A* **1979**, *19*, 1852.
(17) Dufek, P.; Blaha, P.; Schwarz, K. *Phys. Rev. Lett.* **1995**, *75*, 3545.
(18) (a) Lovell, T.; Li, J.; Noodleman, L. *Inorg. Chem*. **2001**, *40*, 5251. (b) Lovell, T.; Li, J.; Noodleman, L. *Inorg. Chem*. **2001**, *40*, 5267.
(19) Lovell, T.; Li, J.; Noodleman, L. *J. Biol. Inorg. Chem*. **2002**, *7*, 799.
(20) te Velde, G.; Bickelhaupt, F. M.; Baerends, E. J.; Fonseca Guerra, C.; van Gisbergen, S. J. A.; Snijders, J. G.; Ziegler, T. *J. Comput. Chem*. **2001**, *22*, 931.

Table 1. Experimental and Predicted Isomer Shifts and Quadrupole Splitting Parameters of Fe Atoms in Polar Monomeric and Dimeric Iron Complexes (RT: Room Temperature)

				exptl					calcd		
complex	CSD ID	ref	oxdn state	T	is	*is*	qs	ref	ND	IS	QS
$Fe(Py)_4Cl_2$	TPYFEC	30	+2	295	1.04	1.16	3.14	31	11 883.18	1.02	2.80
$Fe(bipy)_2Cl_2^+$	CAVDOS05	32	+3	RT	0.42	0.54	0.24	32	11 884.18	0.36	−0.42
FeF_6^{3-}	TUKBOQ	33	+3	297	0.49	0.61	0.38	34	11 883.65	0.71	0.14
$FeCl_6^{3-}$	DALLIL	37	+3	78	0.53	0.56	0.04	38	11 883.91	0.54	−0.07
$FeCl_4^{2-}$	DEBWEM	39	+2	4.2	1.00	1.00	−3.27	40	11 883.18	1.02	3.10
$FeCl_4^-$	MICYFE10	41	+3	RT	0.24	0.36	0.00	32	11 884.48	0.16	−0.12
$Cl_3FeOFeCl_3^{2-}$	FACTEI	42	+3	77	0.33	0.36	1.24	42	11 884.08	0.43	−1.00
			+3	77	0.33	0.36	1.24		11 884.07	0.43	−1.00
$Fe_2O(Oac)_2(HBpz_3)_2$	CACZIP10	43	+3	77	0.52	0.55	1.60	43	11 883.76	0.64	1.5
			+3	77	0.52	0.55	1.60		11 883.73	0.66	1.5
$Fe_2(OH)(OAc)_2(HBpz_3)_2^+$	COCJIN	44	+3	77	0.47	0.50	0.25	43	11 884.06	0.44	0.29
			+3	77	0.47	0.50	0.25		11 884.09	0.42	0.27
$Fe_2O(Oac)_2(Me_3TACN)_2^{2+}$	DIBXAN1 0	45	+3	4.2	0.47	0.47	1.50	45	11 883.91	0.54	1.4
			+3	4.2	0.47	0.47	1.50		11 883.87	0.57	1.4
$Fe_2(OH)(Oac)_2(Me_3TACN)_2^+$	DIBWUG10	44	+2	4.2	1.16	1.16	2.83	44	11 883.00	1.14	3.1
			+2	4.2	1.16	1.16	2.83		11 882.99	1.14	3.1
$Fe_2O(OAc)_2(bipy)_2Cl_2$	VABMUG	46	+3	120	0.37	0.41	1.80	46	11 883.73	0.66	1.2
			+3	120	0.37	0.41	1.80		11 883.72	0.66	1.1
$Fe_2(salmp)_2$	KASFOZ	47	+3	297	0.44	0.56	0.88	48	11 883.76	0.64	1.2
			+3	297	0.44	0.56	0.88		11 883.77	0.63	1.2
$Fe_2(salmp)_2^-$	KASGAM	47	+2.5	297	0.71	0.83	1.08	48	11 883.45	0.84	−0.95
			+2.5	297	0.71	0.83	1.08		11 883.46	0.84	−0.95
$Fe_2(salmp)_2^{2-}$	KASFUF	47	+2	297	0.99	1.11	2.24	48	11 883.16	1.03	1.6
			+2	297	0.99	1.11	2.24		11 883.28	0.96	1.6
$Fe_2BPMP(OPr)_2^+$	GATFOW	49	+3	55	0.48	0.50	0.50	49	11 883.78	0.63	0.95
			+2	55	1.13	1.15	2.69		11 883.12	1.06	3.0
$Fe_2BPMP(OPr)_2^{2+}$	GATFUC	49	+2	55	1.22	1.24	2.72	49	11 883.09	1.08	3.0
			+2	55	1.22	1.24	2.72		11 883.04	1.11	3.0
$Fe_2O_2(6TLA)_2^{2+}$	YOCKAC	50	+3	4.2	0.50	0.50	1.93	51a	11 883.94	0.52	1.5
			+3	4.2	0.50	0.50	1.93		11 883.95	0.51	1.5
$Fe_2O_2(5\text{-}Et_3\text{-}TPA)_2^{3+}$	DEKNO W	51b	+3	4.2	0.14	0.14	0.49	52	11 884.73	0.00	−0.52
			+4	4.2	0.14	0.14	0.49		11 884.71	0.01	−0.52
$Fe_2O(Me_3TACN)_2(Cl_4cat)_2$	YOHMOX	51a	+3	4.2	0.46	0.46	1.41	51a	11 884.03	0.46	−1.3
			+3	4.2	0.46	0.46	1.41		11 884.01	0.47	−1.3
$Fe_2(Cat)_4(H_2O)_2^{2-}$	TEMKUR	53	+3	4.2	0.56	0.56	0.90	53	11 883.78	0.63	−1.1
			+3	4.2	0.56	0.56	0.90		11 883.79	0.62	−1.1

main group atoms C, N, O, and H, which correspond to uncontracted triple-ζ Slater-type orbitals (STO) for the 4s, 4p, and 3d valence orbitals of Fe, triple-ζ STOs for 2s and 2p valence orbitals of C, N, and O augmented with a 3d polarization orbital, and triple-ζ STO for 1s of H with a 2p polarization orbital. The numerical integration scheme was the polyhedron method developed by te Velde et al.[21,22] All calculations used numerical integration accuracy of 4.0, and convergence criteria were set to the ADF2002.02 default parameters. For charged and spin-polarized complexes, such as ligand-bridged diiron systems, antiferromagetic coupling was taken account of by using the broken-symmetry approach used many times before in our laboratory.[23] All calculations employed the spin-unrestricted approach and were done at the GGA level (Vosko−Wilk−Nusair (VWN) parametrization for the LDA)[24] with the generalized gradient correction terms included in the SCF as introduced by Perdew and Wang (PW91) to the exchange and correlation.[25]

2.2. Choice of Polar Monomeric and *μ*-Oxo Dimeric Iron Complexes. Simple polar monomeric iron complexes along with (*μ*-oxo)- and (*μ*-hydroxo)diiron complexes are chosen for the training set as a wide variety of complexes are available to choose from for which isomer shifts and quadrupole splitting parameters are known. The Cartesian coordinates of these structures were extracted directly from the Cambridge structural database. Where hydrogen atoms were not given or were missing in the structures, they were added to the crystal structures using Molden.[26] Our experience shows that partial geometry optimization of all hydrogen atoms in these complexes has only a small effect on the electron densities at the iron nuclei and the electric field gradient. In Table 1, formulas of (*μ*-oxo)diiron complexes are given in abbreviated form, and the full names of the complexes are given in the Appendix. The experimentally determined isomer shifts of iron for the complexes in Table 1 are corrected and correspond to isomer shifts at 4.2 K (italics) by taking account of second-order Doppler effects. The offset given by ($\delta_{4.2K} - \delta_{300K}$) for this correction is 0.12 mm s^{-1}, and this is expected to be linear with temperature.[27]

2.3. Isomer Shifts. HYPER2000[28] is a program to calculate molecular properties of a system on the basis of

(21) Boerrigter, P. M.; te Velde, G.; Baerends, E. J. *Int. J. Quantum Chem*. **1988**, *33*, 87.
(22) te Velde, G.; Baerends, E. J. *J. Comput. Phys*. **1992**, *99*, 84.
(23) Noodleman, L. *J. Chem. Phys*. **1981**, *74*, 5737.
(24) Vosko, S. H.; Wilk, L.; Nusair, M. *Can. J. Phys*. **1980**, *58*, 1200.
(25) Perdew, J. P.; Chekavry, J. A.; Vosko, S. H.; Jackson, K. A.; Perderson, M. R.; Singh, D. J.; Fioihais, C. *Phys. Rev. B* **1992**, *46*, 6671.
(26) Schaftenaar, G.; Noordik, J. H. *J. Comput.-Aided Mol. Des.* **2000**, *14*, 123.
(27) Fee, J. A.; Findling, K. Y.; Yoshida, T.; Hille, R.; Tarr, G. E.; Hearshen, D. O.; Dunham, W. R.; Day, E. P.; Kent, T. A.; Münck, E. *J. Biol. Chem*. **1984**, *259*, 124.

ADF2000 calculations. The nuclear density is calculated using the program HYPERS2000, a subprogram of HYPER2000. The principles employed to calculate the nuclear density are described in Liu et al.[29] Isomer shifts from a given nuclear density are calculated here by

$$\delta = \alpha\{\rho(0) - A\} + C \quad (1)$$

where α is the slope, C is the intercept, and A ($A = 11884.0$) is a constant chosen close to $\rho_s(0)$ (the nuclear density of iron in its reference state). The value of A chosen makes $\rho(0) - A$ a small value. Evaluation of eq 1 is done by linear regression of the experimental isomer shifts, δ versus $\rho(0) - A$, and gives values of α and C for the training set of complexes.

Although the behavior of the electrons in the vicinity of the iron nucleus is influenced by relativistic effects, nonrelativistic wave functions can be used to calculate the electronic charge density at the iron nucleus, because, in the range of interest, the proper relativistic charge density is uniformly higher by a factor of about 1.3 than the charge density calculated without taking into account relativistic effects. To avoid any possible misunderstandings that may arise when comparing the calibration constant α calculated here with that calculated by other workers, reference is only made to the nonrelativistic charge density.

2.4. Quadrupole Splitting Parameters. The energy difference between the two doubly degenerate substates is defined as the quadrupole splitting parameter. The formula for the quadrupole splitting parameter for ^{57}Fe of the nuclear excited state ($I = 3/2$) is

$$\Delta E_Q = {}^1/_2 eQV_{zz}\sqrt{(1 + \eta^2/3)} \quad (2)$$

where e is the electrical charge of a positron, Q with a value of 0.15 barns is the nuclear quadrupole moment, and V is the electric field gradient due to the total electron density plus all nuclear charges. Only off-center nuclear charges contribute to the electric field gradient. V can be decomposed into three principal components, V_{zz}, V_{yy}, and V_{xx}, in descending order of magnitude, and η is the asymmetry parameter defined as $(V_{xx} - V_{yy})/V_{zz}$. The electric field gradient tensors are taken from standard ADF2000 calculations.

3. Results

Experimental Mössbauer parameters[30−53] along with our predicted isomer shifts (IS), quadrupole splitting (QS) parameters, and nuclear densities (ND) for complexes in the training set are presented in Table 1. A plot of experimental isomer shift δ versus $\rho(0)$ is shown in Figure 1; calculated versus experimental quadrupole splitting parameters are shown in Figure 2. In the table, experimental isomer shifts and quadrupole splittings that are designated "is" and "qs", respectively, correspond to those reported in the literature at temperature T; experimental isomer shifts designated "*is*" are corrected for second-order Doppler shift to 4.2 K.

3.1. Linear Relationship for Isomer Shifts for Synthetic Systems. Linear regression of the experimental isomer shifts versus the corresponding $\rho(0) - 11884.0$ gives values for α and C in Table 2 along with other properties for this fit. Most importantly, the correlation coefficient (r) is -0.94 and the standard deviation (SD) of the fit is 0.11 mm s^{-1}. The fit quality is comparable to that noted previously by Liu et al.[29] for iron−sulfur-based systems. For six out of seven cases in the monomeric systems, the calculated isomer shift and experimental isomer shift corrected to 4.2 K are in remarkably good agreement with each other. The worst correlation is for $FeCl_4^-$, where the calculated isomer shift is too small by 0.2 mm s^{-1}. For the dinuclear systems, the correlation for 13 of the complexes is also very good; the worst of the 14 cases examined is in error by 0.25 mm s^{-1}.

For more than 20 years, there has been continuing uncertainty over the correct value of the calibration constant α. Two recent articles from Zhang et al.[54] and Neese[55] have been prominent in this area. In both articles, DFT calculations of similar quality are reported, which however lead to

(28) Liu, T.; Case, D. A.; Noodleman, L. Manual of Hyper2000, 2000; Internal Report of the Scripps Research Institute.
(29) Liu, T.; Lovell, T.; Ullmann, G. M.; Case, D. A.; Noodleman, L. *Inorg. Chem.*, submitted for publication.
(30) Long, G. J.; Clark, P. J. *Inorg. Chem.* **1978**, *17*, 1394.
(31) Burbridge, C. D.; Goodgame, D. M. L.; Goodgame, M. *J. Chem. Soc. A* **1967**, 349.
(32) Witten, E. H.; Reiff, W. M.; Lazar, K.; Sullivan, B. W.; Foxman, B. M. *Inorg. Chem.* **1985**, *24*, 4585.
(33) Rother, G.; Worzala, H.; Bentrup, U. *Z. Anorg. Allg. Chem.* **1991**, *622*, 443.
(34) Wertheim, G. K.; Guggenheim, H. J.; Buchanan, D. N. E. *Phys. Rev.* **1968**, *169*, 465.
(35) Arutyunyan, L. D.; Ponomarev, V. I.; Atovmyan, L. O.; Lavrent'ev, E. A.; Khidekel, M. L. *Koord. Khim.* **1979**, *5*, 943.
(36) Pfletschinger, E. *Z. Phys.* **1968**, *209*, 119.
(37) Damant, U.; Conradi, E.; Muller, U.; Dehnicke, K. *Z. Naturforsch., B* **1985**, *40*, 443.
(38) Earls, D. E.; Axtmann, R. C.; Hazony, Y.; Lefkowitz, I. *J. Phys. Chem. Solids* **1968**, *29*, 1859.
(39) Schmid, G.; Barbenheim, G.; Boese, R. *Z. Naturforsch., B* **1985**, *40*, 787.
(40) Coucouvanis, D.; Greiwe, K.; Salifoglou, A.; Challen, P.; Simopoulos, A.; Kostikas, A. *Inorg. Chem.* **1988**, *27*, 594.
(41) Constant, G.; Daran, J.-C.; Jeannin, Y. *J. Inorg. Nucl. Chem.* **1973**, *35*, 4083.
(42) Petridis, D.; Terzis, A. *Inorg. Chim. Acta* **1986**, *118*, 129.
(43) Armstrong, W. H.; Spool, A.; Papaefthymiou, G. C.; Frankel, R. B.; Lippard, S. J. *J. Am. Chem. Soc.* **1984**, *106*, 3653.
(44) Armstrong, W. H.; Lippard, S. J. *J. Am. Chem. Soc.* **1984**, *106*, 4632.
(45) Hartman, J. A. R.; Rardin, R. L.; Chaudhuri, P.; Pohl, K.; Wieghardt, K. Nuber, B.; Weiss, J.; Papaefthymiou, G. C.; Frankel, R. B.; Lippard, S. J. *J. Am. Chem. Soc.* **1987**, *109*, 7387.
(46) Vincent, J. B.; Hoffman, J. C.; Christou, G.; Li, Q.; Nanny, M. A.; Hendrickson, D. N.; Fong, R. H.; Fish, R. H. *J. Am. Chem. Soc.* **1988**, *110*, 6898.
(47) Snyder, B. S.; Patterson, G. S.; Abrahamson, A. J.; Holm, R. H. *J. Am. Chem. Soc.* **1989**, *111*, 5214.
(48) Surerus, K. K.; Münck, E.; Snyder, B. S.; Holm, R. H. *J. Am. Chem. Soc.* **1989**, *111*, 5501.
(49) Borovik, A. S.; Que, L., Jr. *J. Am. Chem. Soc.* **1988**, *110*, 2345.
(50) Zang, Y.; Dong, Y.; Que, L., Jr.; Kauffmann, K.; Münck, E. *J. Am. Chem. Soc.* **1995**, *117*, 1169.
(51) (a) Justel, T.; Weyhermuller, T.; Wieghardt, K.; Bill, E.; Lengen, M.; Trautwein, A. X.; Hildbrandt, P. *Angew. Chem., Int. Ed. Engl.* **1995**, *34*, 669. (b) Hsu, H.-F.; Dong, Y.; Shu, L.; Young, V. G., Jr.; Que, L., Jr. *J. Am. Chem. Soc.* **1999**, *121*, 5230.
(52) Dong, Y.; Fujii, H.; Hendrich, M. P.; Leising, R. A.; Pan, G.; Randall, C. R.; Wilkinson, E. C.; Zhang, Y.; Que, L., Jr.; Fox, B. G.; Münck, E. *J. Am. Chem. Soc.* **1995**, *117*, 2778.
(53) Grillo, V. A.; Hanson, G. R.; Wang, D.; Trevor, T. W.; Hambley, W.; Gahan, L. R.; Murray, K. S.; Moubaraki, B.; Hawkins, C. J. *Inorg. Chem.* **1996**, *35*, 3568.
(54) Zhang, Y.; Mao, J.; Oldfield, E. *J. Am. Chem. Soc.* **2002**, *124*, 7829.
(55) Neese, F. *Inorg. Chim. Acta* **2002**, *337*, 181.

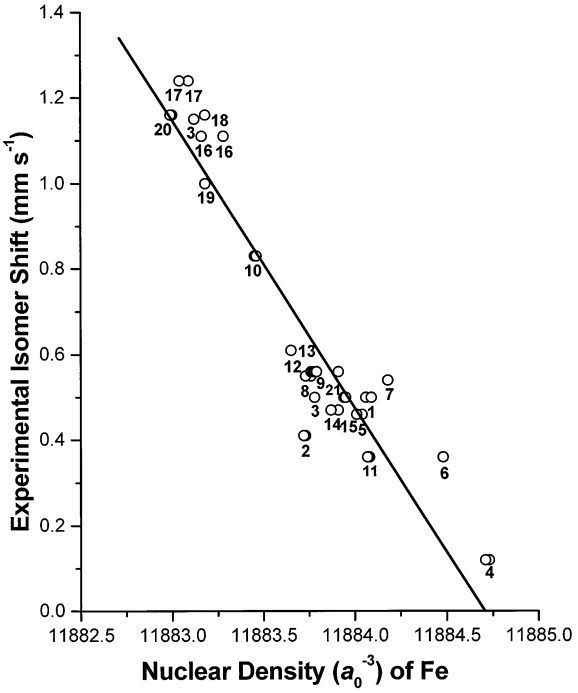

Figure 1. Plot of calculated nuclear density versus experimental isomer shift for a series of synthetic mononuclear and dinuclear iron complexes. Key: 1, $Fe_2(OH)(OAc)_2(HBpz_3)_2^+$; 2, $Fe_2O(OAc)_2(bipy)_2Cl_2$; 3, $Fe_2(BPMP)(OPr)_2^{2+}$; 4, $Fe_2O_2(5\text{-}Et_3\text{-}TPA)_2^{3+}$; 5, $Fe_2O(Me_3TACN)_2(Cl_4cat)_2$; 6, $FeCl_4^-$; 7, $Fe(bipy)_2Cl_2^+$; 8, $Fe_2(salmp)_2$; 9, $Fe_2(Cat)_4(H_2O)_2^{2-}$; 10, $Fe_2(salmp)_2^-$; 11, $Cl_3FeOFeCl_3^{2-}$; 12, FeF_6^{3-}; 13, $Fe_2O(OAc)_2(HBpz_3)_2$; 14, $Fe_2O(OAc)_2(Me_3TACN)_2^{2+}$; 15, $Fe_2O_2(6TLA)_2^{2+}$; 16, $Fe_2(salmp)_2^{2-}$; 17, $Fe_2(BPMP)(OPr)_2^+$; 18, $Fe(Py)_4Cl_2$; 19, $FeCl_4^{2-}$; 20, $Fe_2(OH)(OAc)_2(Me_3TACN)_2^+$; 21, $FeCl_6^{3-}$.

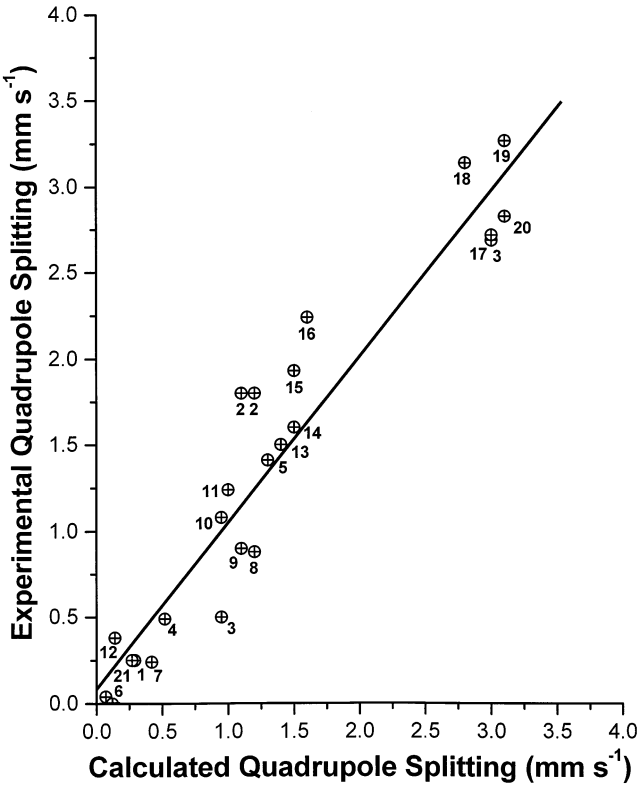

Figure 2. Plot of calculated quadrupole splitting versus experimental quadrupole splitting for a series of synthetic mononuclear and dinuclear iron complexes. Key: 1, $Fe_2(OH)(OAc)_2(HBpz_3)_2^+$; 2, $Fe_2O(OAc)_2(bipy)_2Cl_2$; 3, $Fe_2(BPMP)(OPr)_2^{2+}$; 4, $Fe_2O_2(5\text{-}Et_3\text{-}TPA)_2^{3+}$; 5, $Fe_2O(Me_3TACN)_2(Cl_4cat)_2$; 6, $FeCl_4^-$; 7, $Fe(bipy)_2Cl_2^+$; 8, $Fe_2(salmp)_2$; 9, $Fe_2(Cat)_4(H_2O)_2^{2-}$; 10, $Fe_2(salmp)_2^-$; 11, $Cl_3FeOFeCl_3^{2-}$; 12, FeF_6^{3-}; 13, $Fe_2O(OAc)_2(HBpz_3)_2$; 14, $Fe_2O(OAc)_2(Me_3TACN)_2^{2+}$; 15, $Fe_2O_2(6TLA)_2^{2+}$; 16, $Fe_2(salmp)_2^{2-}$; 17, $Fe_2(BPMP)(OPr)_2^{1+}$; 18, $Fe(Py)_4Cl_2$; 19, $FeCl_4^{2-}$; 20, $Fe_2(OH)(OAc)_2(Me_3TACN)_2^+$; 21, $FeCl_6^{3-}$.

significantly different values for α. Depending on the applied computational method, Zhang et al. obtained −0.3471 au (Using Hartree−Fock), −0.4108 au (B3LYP), and −0.4771 au (BPW91), whereas Neese obtained −0.366 au (B3LYP) and −0.402 au (BP86). Previous work in our laboratory gave calibration constants of −0.51 for iron−sulfur complexes[56] and −0.47 for a broader range of iron complexes with the same BP86 potential,[29] using the ADF codes and triple-ζ Slater type basis sets on iron. These values can be compared with $\alpha = -0.66$ in the current work using a similar quality basis set and the PW91 potential. As pointed out by Neese, the obtained value for α depends on the method and basis sets chosen, as well as on the training set of molecules. While in principle an exact value of α exists, whose value is not known, in practice, there may be many different exchange-correlation potentials with different predicted α values, which are of good and sufficient accuracy so long as the correlation is high and reliable.

In a comparison of the results from Zhang et al.[54] and Neese[55] with those of this work and our earlier work, there is a trend to smaller calibration constants when going from pure density functionals (also where PW91 > BPW91 > BP86) to hybrid functionals (B3LYP) and to the pure Hartree−Fock method (HF). The increased inclusion of HF exchange is the main reason for the decrease of α, with the choice of molecules in the training set and the numerical methods employed playing a smaller but significant role.

Table 2. Isomer Shift (IS) Correlation Linear Regression and Quadrupole Splitting Parameters (QS) Comparisons: Slopes (α); Intercepts (*C*); Number of Fitting Points (*N*); Standard Deviations (SD); Coefficients of Correlation (*r*)

param	IS fitting	QS comparisons
α	−0.664 ± 0.04	0.96 ± 0.03
C	0.478 ± 0.02	0.12 ± 0.02
r	−0.94	0.95
SD	0.11	0.12
$\rho_s(0)$	11 884.72 ± 0.07	
N	36	36

3.2. Comparisons of Quadrupole Splitting Parameters for Synthetic Systems. The direct rms deviation between calculated and observed quadrupole splittings is 0.3 mm s^{-1} prior to the linear fitting. Linear regression of the quadrupole splitting plot is based on the following equation:

$$QS_{expt} = \alpha QS_{calc} + C \qquad (3)$$

The parameters for the fit and the standard deviation between calculated and experimental quadrupole splitting parameters are shown in Table 2. As noted for the isomer shifts, calculated quadrupole splittings in Table 1 are also in very good agreement with the experimental values for monomeric and dimeric iron systems. Most importantly, the correlation

(56) (a) Lovell, T.; Li, J.; Liu, T.; Case, D. A.; Noodleman, L. *J. Am. Chem. Soc.* **2001**, *123*, 12392. (b) Lovell, T.; Liu, T.; Case, D. A.; Noodleman, L. *J. Am. Chem. Soc*. **2003**, *125*, 8377.

Table 3. Model Compounds of MMOH: Calculated (Isomer Shifts (IS), Nuclear Densities (ND), Quadrupole Splitting Parameters (QS), Asymmetry Factors (η)) and Experimental (Isomer Shifts (*is*), Quadrupole Splittings (qs)) Parameters with Isomer Shifts and Quadrupole Splittings in mm s^{-1} (AF, Antiferromagnetic; F, Ferromagnetic)

			isomer shift				quadrupole splitting			
model	charge	site	ND	IS	*is*	ref	QS	η	qs[f]	ref
					Oxidized MMOH Fe^{III} Fe^{III}					
AF C_i[a]	1	Fe_1	11 883.69	0.68	0.47	61[g]	−0.87	0.37	1.46	61
		Fe_2	11 883.53	0.79	0.72	61	−1.0	0.49	1.33	61
AF D[b]	0	Fe_1	11 883.67	0.70	0.50	57, 58	−1.0	0.42	1.12, 1.16	57, 58
		Fe_2	11 883.77	0.63	0.51	57, 58	0.43	0.02	0.79, 0.87	57, 58
X-ray[c]	1	Fe_1	11 883.18	1.02			−1.7	0.85		
		Fe_2	11 883.61	0.74			−2.3	0.52		
X-ray[d]	0	Fe_1	11 883.08	1.09			−1.7	0.90		
		Fe_2	11 883.70	0.68			−1.0	0.80		
					Reduced MMOH Fe^{II} Fe^{II}					
F B[e]	0	Fe_1	11 882.43	1.52	1.3	57, 58	3.2	0.29	3.1, 3.01	57, 58
		Fe_2	11 882.57	1.43	1.3	57, 58	2.5	0.39	2.4−3.0	57, 58
AF B	0	Fe_1	11 882.40	1.54			3.3	0.05		
		Fe_2	11 882.58	1.42			2.7	0.31		
X-ray	0	Fe_1	11 882.55	1.44			3.2	0.24		
		Fe_2	11 882.51	1.47			3.5	0.46		

[a] Oxidized model containing bridging hydroxide and water ligands from ref 18. [b] Oxidized model containing two bridging hydroxide ligands from ref 18. [c] From *M. capsulatus* 1MTY structure from the PDB. [d] From *M. trichosporium* 1MHY structure from the PDB from ref 5a. [e] Reduced model from ref 18 and X-ray coordinates obtained from personal communication, Steve Lippard's group, MIT. [f] For the MMOH quadrupole splittings, the first value is for *M. capsulatus* and the second for *M. trichosporium*. [g] For *M. capsulatus*.

Table 4. Model Compounds of RNR: Calculated (Isomer Shifts (IS), Nuclear Densities (ND), Quadrupole Splitting Parameters (QS), Asymmetry Factors (η)) and Experimental (Isomer Shifts (*is*), Quadrupole Splittings (qs)) Parameters with Isomer Shifts and Quadrupole Splittings in mm s^{-1} (AF, Antiferromagnetic; F, Ferromagnetic)

			isomer shift				quadrupole splitting			
model	charge	site	ND	IS	*is*	ref	QS	η	qs	ref
					Oxidized RNR Fe^{III} Fe^{III}					
AF[a]	0	Fe_1	11 883.55	0.78	0.45	59, 60[e]	−1.2	0.61	2.44	59, 60
		Fe_2	11 883.43	0.86	0.55	59, 60	−1.5	0.93	1.62	59, 60
X-ray[b]	0	Fe_1	11 883.09	1.08			0.83	0.38		
		Fe_2	11 883.14	1.05			1.10	0.63		
					Reduced RNR Fe^{II} Fe^{II}					
F	0	Fe_1	11 882.80	1.28			2.4	0.44		
		Fe_2	11 883.30	0.94			−1.2	0.68		
AF[c]	0	Fe_1	11 882.77	1.30	1.26	59, 60	2.6	0.42	3.13	59, 60
		Fe_2	11 883.28	0.96			−1.4	0.85		
X-ray[d]	0	Fe_1	11 883.16	1.04			3.0	0.48		
		Fe_2	11 884.14	0.38			1.4	0.97		

[a] Oxidized model from ref 19. [b] *E. coli* 1RIB structure from PDB from ref 63a. [c] Reduced model from ref 19. [d] *E. coli* 1XIK structure from the PDB from ref 63b. [e] Experimental results assigned to only one site.

coefficient is high, $r = 0.95$, the slope of the fit $\alpha = 0.96$ is near the ideal value $\alpha_{ideal} = 1$, and SD = 0.12 mm s^{-1}. This level of accuracy in predicting quadrupole splitting parameters is likely to be very valuable to help to distinguish between structurally characterized and uncharacterized models for the active sites of binuclear non-heme iron proteins. The high level of correlation between predicted and experimental parameters also gives us confidence that our established correlation should work reasonably well for iron−oxo-containing active sites of proteins.

3.3. Applications to Methane Monooxygenase and Ribonucleotide Reductase. Isomer shifts and quadrupole splitting parameters for the iron sites in the oxidized and reduced hydroxylase component of MMO are given in Table 3,[57,58] while those for oxidized and reduced RNR are given in Table 4.[59,60] Where the ferromagnetic and antiferromagnetic states lie close in energy, as is the case in the reduced states, both are shown. In both tables, isomer shift and quadrupole splitting parameters are calculated at the experimental geometry and after geometry optimization. It is immediately obvious that the calculated isomer shifts for active site in both proteins evaluated at the experimental geometries are much higher than the measured values;[57,58,59,60] this discrepancy improves somewhat upon geometry optimization, as the calculated nuclear density shows a clear dependence upon geometry, but nevertheless, the calculated isomer shifts are still too high compared to experiment.

From a single turnover of *M. capsulatus*, two sets of isomer shift measurements have been obtained for the

(57) Fox, B. G.; Hendrich, M. P.; Surerus, K. K.; Anderson, K. K.; Froland, W. A.; Lipscomb, J. D.; Münck, E. *J. Am. Chem. Soc*. **1993**, *115*, 3688.

(58) DeWitt, J. G.; Dentsen, J. G.; Rosenzweig, A. C.; Hedman, B.; Green, J.; Pilkington, S.; Papaefthymiou, G. C.; Dalton, H.; Hodgson, K. O.; Lippard, S. J. *J. Am. Chem. Soc*. **1991**, *113*, 9219.

(59) Atkin, C. L.; Thelander, L.; Reichard, P.; Lang G. *J. Biol. Chem*. **1973**, *248*, 7464.

(60) Lynch, J. B.; Juarez-Garcia, C.; Münck, E.; Que, L., Jr. *J. Biol. Chem*. **1989**, *264*, 8091.

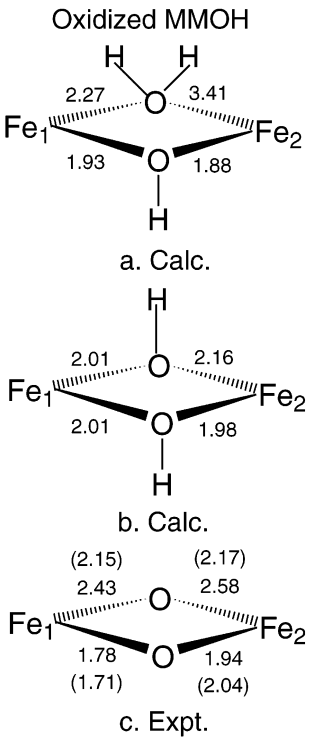

Figure 3. Calculated (a, b)[18] and X-ray experimental distances (c) from *M. capsulatus*[4] and *M. trichosporium*[5a] (in parentheses) of core structures in the hydroxylase component of oxidized methane monooxygenase. The calculated structure (a) corresponds to model C tautomer I and (b) to model D (see ref 18).

oxidized hydroxylase active site of MMO[10,61] indicating the presence of two structures for the binuclear ferric cluster. The first is characterized by two equal intensity quadrupole doublets, with $\Delta E_Q = 1.12$ and 0.79 mm s^{-1} and $\delta = 0.51$ and 0.50 mm s^{-1}. The second exhibits two doublets with $\Delta E_Q = 1.46$ and 1.33 mm s^{-1} and $\delta = 0.72$ and 0.47 mm s^{-1}. It is difficult to evaluate whether the heterogeneity observed in the single-turnover Mössbauer measurements can be correlated with structural heterogeneity from the X-ray crystallographic analysis. One should consider also the set of larger isomer shift values (0.72 and 0.47 mm s^{-1}) in comparison with the calculations, where the difference in isomer shifts between the two sites in the secondary species is better reproduced. On this basis, in accord with experimental observations, we cannot dismiss the set of larger values, particularly as the average of these values (0.60 mm s^{-1}) exceeds the average for the first and more typical species widely referred to in the literature (0.51 mm s^{-1}). The isomer shifts for *M. trichosporium* are very near those reported for *M. capsulatus*, 0.50−0.51 mm s^{-1}, and reported quadrupole splittings are similar (see Table 3).

Generally though, the isomer shifts depend on the nature and geometry of ligands surrounding each iron site, their donor abilities, and the distances of ligands. More specifically, for oxidized MMOH in Figure 3, the Mössbauer isomer shifts appear sensitive to the oxygen donors, particularly to the closest OH^- ligand. X-ray structures (Figure 3c) give too short a distance for the closest Fe−OH^- interaction, which appears more Fe−O^{2-} like.[18] In agreement with our calculations and analysis[18] (Figure 3a,b), it is clear from optical spectroscopy[58] that one or both of the bridging ligands must be hydroxide and none are oxo. Both the direct effect from OH^-donation and indirect effects from donation of other O and N centers in the local coordination vicinity will influence Mössbauer parameters, which for our optimized geometries, although not perfect, are clearly better than for the experimental geometries.

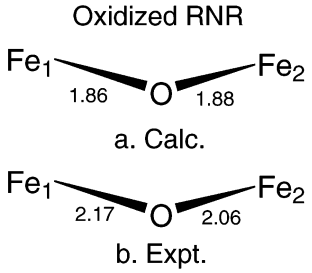

Figure 4. Calculated (a)[19] and X-ray experimental distances (b) from *E coli* of core structures in oxidized ribonucleotide reductase.[63a]

For oxidized RNR, our calculations (Figure 4a) along with resonance Raman spectroscopy[62] indicate a single oxo bridge along with a bridging carboxylate. The X-ray structure geometry (Figure 4b) is much longer and more appropriate to a water bridge. Again, calculated isomer shifts are better for the optimized structures compared to the experimental structures and, clearly, there are remaining discrepancies which are larger for RNR than MMOH (see Tables 3 and 4). The average deviation of calculated isomer shifts from experiment are 0.17 to 0.20 mm s^{-1} ($MMOH_{ox}$), 0.32 mm s^{-1} (RNR_{ox}), 0.17 mm s^{-1} ($MMOH_{red}$), and 0.17 mm s^{-1} (RNR_{red}) using calculated optimized geometries. The standard deviation of the training set of synthetic complexes of well-defined structures is smaller at 0.11 mm s^{-1}.

Given the limited resolution of the X-ray data for these metalloproteins, which ranges from 1.7 to 2.2 Å, it is not surprising that there may be additional geometric uncertainties in the current best X-ray-derived geometries. Additionally, there may be electronic influences from the longer range environment. Both factors may serve to regulate charge-transfer effects from ligand to metal and alter isomer shifts.

A related trend occurs in the calculated quadrupole splitting parameters for oxidized MMOH, which are also calculated much larger at the X-ray coordinates.[63] After geometry optimization, the calculated values improve somewhat toward those measured experimentally with those for oxidized MMOH appearing in pretty good agreement with the reported experimental values. Shorter and stronger oxygen coordination from oxo or hydroxyl ligands is typically associated with larger quadrupole splittings experimentally,[64] and this same trend can be seen in the calculated

(61) Liu, K. E.; Valentine, A. M.; Wang, D.; Huynh, B.-H.; Edmondson, D. E.; Salioglou, A.; Lippard, S. J. *J. Am. Chem. Soc*. **1995**, *117*, 10174.

(62) Sjöberg, B.-M.; Loehr, T. M.; Sanders-Loehr, J. *Biochemistry* **1982**, *21*, 96.

(63) Nordlund, P.; Eklund, H. *J. Mol. Biol*. **1993**, *232*, 123. (b) Logan, D. T.; Su, X.-D.; Aberg, A.; Regnstrom, K.; Hajdu, J.; Eklund, H.; Nordlund, P. *Structure* **1996**, *4*, 1053.

(64) Lynch, J. B.; Juarez-Garcia, C.; Münck, E.; Que, L., Jr. *J. Biol. Chem*. **1989**, *264*, 8091.

quadrupole splittings comparing DFT geometry optimized to the X-ray structure values in both oxidized MMOH and RNR.

The largest difference in ΔE_Q is found for one iron site (bonded to Asp84) in oxidized RNR where the experimental quadrupole splitting of 2.45 mm s^{-1} deviates considerably from the calculated value of 1.2 mm s^{-1} and is quite atypical for an iron(III) site in a diferric oxo-bridged system. This is evident from Table 1 and Figure 2 where $Fe_2O_2(6TLA)_2^{2+}$ (complex 15) has the highest ΔE_Q (1.93 mm s^{-1}) among all the synthetic diferric systems. This anomaly for ΔE_Q in oxidized RNR was also commented on in an experimental review paper by Huynh et al.,[10] where it was proposed this may be due to bidentate binding of Asp84 to the iron site nearest tyrosine 122 (note also the influence of a strong oxo bridge discussed above). In contrast, the 2.2 Å resolution X-ray structure gives quite asymmetric Fe1−AspOδ1 and Fe1−AspOδ2 distances of 2.16 and 2.52 Å, respectively, and our DFT calculations give a local minimum at a similar iron site geometry.

3.4. Concluding Remarks. There is a significant contrast between the DFT-predicted and experimentally observed isomer shift and quadrupole splitting parameters for synthetic complexes in the training set and for the structurally characterized active sites of MMO and RNR. This difference is considerably larger for oxidized RNR than for oxidized MMOH and for their reduced equivalents, RNR_{red} and $MMOH_{red}$, which display uncertainties closer to those in the training set. The linear relationship between isomer shifts and calculated nuclear density for a wide variety of synthetic mononuclear and dinuclear iron complexes seems reliable, and the correlation appears to be very good in the case of the high-resolution, small-molecule training set. However, when we apply the same correlation to the case of the structurally characterized protein active sites of MMO and RNR, significant differences arise in our predicted isomer shifts for oxidized MMOH and RNR; they are, in all cases, calculated too high.

There are a number of possible rational explanations for this. First, the most obvious is that DFT calculations are not without structural and electronic errors. However, the predicted isomer shifts and quadrupole splittings for the synthetic complexes suggest the calculations behave in an overall reliable fashion. These fits to the synthetic models were used recently in fitting calculated Mössbauer parameters to a potential model for intermediate Q of MMO.[65] The protein active site molecules are intrinsically more complicated and with greater structural uncertainties. Structural uncertainties appear largest in oxidized RNR, where Tyr122−Asp84 hydrogen bonding and monodentate versus bidentate Asp84-to-iron coordination is an issue. For oxidized MMOH and RNR protein active sites, the position of the bridging oxo in oxidized RNR and bridging hydroxo in oxidized MMOH appears to be particularly important.

Second, the resolution of the protein structural data in the worst case for oxidized RNR is 2.2 Å. At this level of resolution, the assignment of accurate bond distances and angles can be, at best, only approximate, and large degrees of structural uncertainty associated with bond distances would not be uncommon. Geometry optimization of these structures remedies the situation somewhat, but the calculated Mössbauer isomer shift parameters are still too large.

Third, the recent structure of nitrogenase of resolution 1.1 Å[66] has revealed the considerable added value of having a very high resolution structure on which to base DFT calculations. Prior to this, the best previous structure of nitrogenase was only resolved to 1.6 Å. The increased resolution of 0.5 Å revealed the presence of a atom in the center of the active site that was previously unseen, and this will no doubt have a profound effect upon the properties of the nitrogenase active site.[56b] It is therefore also possible that higher resolution structures for the oxidized and reduced states of the MMO and RNR when obtained may reveal previously unseen aspects of these protein structures. For instance, it is well-known that the carboxylate groups of aspartate and glutamate side chains are highly flexible both in the orientation and coordinate modes across the family of binuclear non-heme iron proteins. Thus, if aspartate84 is bidentate and not monodentate as is suggested in the 2.2 Å X-ray structure of oxidized RNR, the differing coordination mode of the carboxylate group will no doubt have an effect on the calculated isomer shift and quadrupole splitting of that iron site. Flexible and/or highly variable site geometries are almost certain to be present for a number of states of the catalytic cycles of MMO and RNR, and additional DFT calculations over a variety of conformations are planned to further examine these issues.

Appendix: Abbreviations

The following abbreviations are used:
Py, pyridine;
bipy, 2,2′-bipyridine;
Oac, acetate;
$HBPz_3$, hydrotris(pyrazolyl)borate;
salmp, 2-bis(saliclideneamino)methylphenol;
BPMP, 2,6-bis[bis(2-pyridylmethyl)aminomethyl]-4-methylphenol;
OPr, propionate;
6TLA, tris(6-methylpyridyl-2-methyl)amine;
TPA, tris(2-pyridylmethyl)amine;
cat, catecholate.

Acknowledgment. We appreciate the very helpful comments provided by the two reviewers of this manuscript. This work was supported by NIH Grant GM 43278 to L.N. We also thank the Amsterdam group for the use of the ADF codes.

IC020640Y

(65) Lovell, T.; Han, W.-G.; Liu, T.; Noodleman, L. *J. Am. Chem. Soc.* **2002**, *124*, 5890.
(66) Einsle, O.; Tezcan, F. A.; Andrade, S. L. A.; Schmid, B.; Yoshida, M.; Howard, J. B.; Rees, D. C. *Science* **2002**, *297*, 1696.